ADVANCED MATERIALS

DOI: 10.1002/adma.200602396

Nanosheet-Based Microspheres of Eu^{3+}-doped ZnO with Efficient Energy Transfer from ZnO to Eu^{3+} at Room Temperature**

By *Xiaoyan Zeng*,* *Junlin Yuan*, *Zhenyang Wang*, and *Lide Zhang**

Rare earth (RE^{3+})-doped semiconductors, such as GaN:RE[1] and Si:Er,[2] are technologically important materials in optoelectric devices and have received considerable interest. In most of these applications, efficient energy transfer from host to the RE^{3+} is desired. ZnO with a bandgap of 3.37 eV and a bound exciton energy of 60 meV is also an important semiconductor for which UV,[3] blue,[4] and green[5] emissions are widely reported, but intense red emissions are still lacking. Among the RE^{3+} activators, the red $^5D_0$–$^7F_2$ emission of Eu^{3+} is widely used in light-emitting devices. Unfortunately, the work of harvesting intense Eu^{3+} emission from ZnO films, ceramics, and powders remains disappointing[6] because of the strong quenching effect of the wide-band, self-activated, green or yellow emissions and the higher energy-level position of Eu^{2+} relative to the bottom conduction band (CB).[7] It has been established that direct ZnO→Eu^{3+} energy transfer seems physically impossible, as the radiative and nonradiative decay of excitons in ZnO are $>10^2$ times faster than the energy-transfer rate of RE^{3+}.[8] Fortunately, energy transfer can be facilitated by the presence of intrinsic or extrinsic defects as energy trap centers in various systems, such as SiC:(N, Er), ZnO:(N, Eu), and ZnO:(F, Eu),[9] which suggests that the introduction of an appropriate trap center is crucial for efficient ZnO→Eu^{3+} energy transfer.

The trap center might be introduced in ZnO nanostructures where surface defects may play a key role in electrical and optical processes.[10] Among the reported ZnO:Eu^{3+} nanostructures fabricated via wet chemical routes, none have shown efficient ZnO→Eu^{3+} energy transfer, partly because it is difficult to insert Eu^{3+} ions into wurtzite ZnO nanocrystals that grow along the c-axis.[11] In other words, the efforts of fabricating ZnO:Eu^{3+} nanostructures with efficient ZnO→Eu^{3+} energy transfer have been unsuccessful.

In this work, we fabricated nanosheet-based microspheres of ZnO:Eu via a hydrothermal strategy involving the formation of a layered hydroxide zinc carbonate (LHZC), $Zn_5(OH)_6(CO_3)_2$, and further heat treatment. For the first time, efficient ZnO→Eu^{3+} energy transfer at room temperature was observed, and intense red Eu^{3+} emission that would be very useful in full color displays was obtained from ZnO nanostructures.

The fabrication strategy was initiated by Hosono et al.,[12] who first fabricated layered hydroxide zinc salt (LHZS) nanosheets as self-template precursors; porous ZnO nanosheets were obtained after heat treatment. This strategy is advantageous over the conventional growth of wurtzite ZnO nanocrystals into which large RE^{3+} ions are doped because 3/5 of the Zn^{2+} ions stay in [ZnO_6] octahedra (average $d_{Zn\text{-}O}$ = 0.2106 nm) rather than in [ZnO_4] tetrahedra (average $d_{Zn\text{-}O}$ = 0.1978 nm in ZnO).[13] In the hydrothermal process, Zn^{2+} ions first react with the OH^- and CO_3^{2-} released by urea to form an insoluble LHZC (Fig. 1a) at the bottom of the autoclave, which is decomposed into wurtzite ZnO after further annealing at 400 °C (Fig. 1b). It is worth noting that the saturated concentration of Eu^{3+} in ZnO is relatively low, smaller than 1.0 % (ca. 4.2×10^{26} cm^{-3}). As shown in Fig. 1b and c, if the starting concentration of Eu^{3+} is higher than 1.0 %, the excess Eu^{3+} ions will remain outside of ZnO in the form of amorphous hydroxide europium carbonate (low temperature, 400 °C) or crystalline Eu_2O_3 (high temperature, 700 °C) (see Supporting Information, Fig. 1s). In addition, no meaningful shift in the X-ray diffraction (XRD) peaks for ZnO were detected, which indicates a low concentration of Eu^{3+} in ZnO. Nevertheless, the X-ray photoelectron spectroscopy (XPS) 3d spectrum for Eu provides convincing evidence for Eu^{3+} doping in ZnO (see Supporting Information, Fig. 2s). Consequently, in samples for optical measurements, the starting concentration of Eu^{3+} was lower than 1.0 % to exclude the disturbance from the Eu^{3+} ions outside of ZnO.

Hosono et al.[12] proposed that LHZC follows a sheetlike growth feature along the hydrophilic b- and c-axes, whereas the (100) surface is hydrophobic. We describe the mechanism for the nucleation and crystal growth of LHZC microspheres as follows: after homogenous nucleation in solution, nuclea-

[*] Dr. X. Y. Zeng, Prof. L. D. Zhang, Dr. Z. Y. Wang
Key Laboratory of Materials Physics, Institute of Solid state Physics
Graduate School of the Chinese Academy of Science
Chinese Academy of Sciences
P. O. Box 1129, Hefei 230031 (P. R. China)
E-mail: xyzeng@issp.ac.cn, ldzhang@issp.ac.cn
Dr. J. L. Yuan
State Key Laboratory of High Performance Ceramics and Superfine Microstructures
Shanghai Institute of Ceramics
Chinese Academy of Sciences
1295 Dingxi Road, Shanghai 200050 (P. R. China)

[**] This work was financially supported by the National Major Project of Fundamental Research: Nanomaterials and Nanostructures (Grant no. 2005CB623603) and the Natural Science Foundation of China (Grant No. 10304018). We also thank Dr. C. H. Ye and Dr. H. B. Zeng for helpful discussions and advice. Supporting Information is available online from Wiley InterScience or from the author.

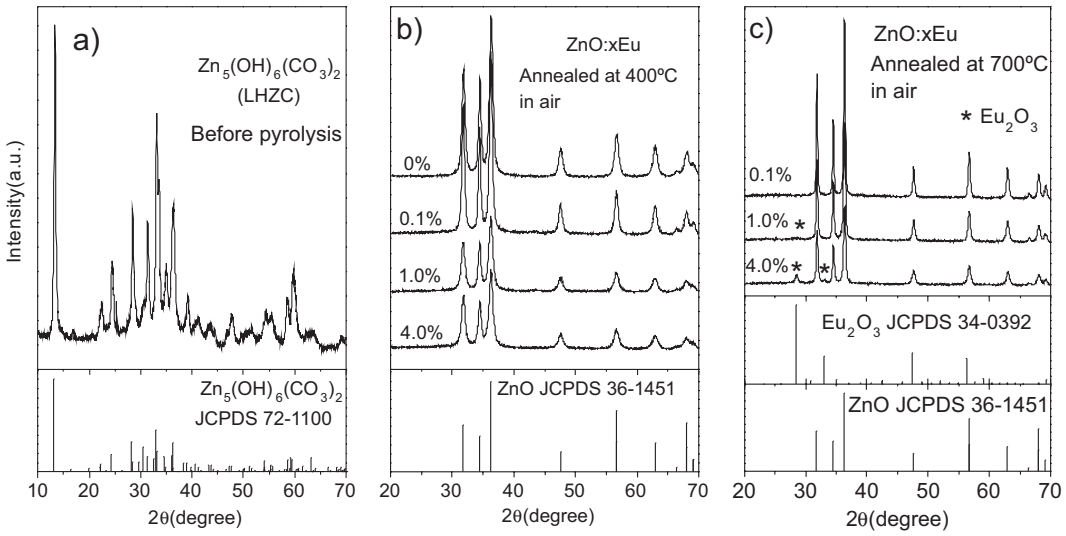

Figure 1. XRD patterns of a) hydrothermal products before heat treatment and ZnO:*x* Eu (*x* = 0, 0.1 %, 1.0 %, 4.0 %) samples annealed at b) 400 °C and c) 700 °C in air. The concentrations of Eu^{3+} are atomic starting concentrations.

tion and crystal growth happen at the edges of LHZC nanosheets, which finally leads to the formation of microspheres of closely stacked LHZC nanosheets because of the steric hindrance between nanosheets (Fig. 2a). During the subsequent pyrolysis, the LHZC nanosheet converts to a 10–25 nm thick mesoporous ZnO nanosheet (Fig. 2b and c), in which ZnO nanocrystals (ca. 4 nm)[12b] grow into larger single crystals along the [0001] direction (Fig. 2d and e). The ZnO:Eu nanosheet, which extends in the plane of the [001] and [110] axes such that most of the surface belongs to the [1$\bar{1}$00] crystal plane, is of high crystalline quality (Fig. 2e), except for irregular pores with estimated diameters of 10–30 nm (Fig. 2d) that were also formed during the pyrolysis and crystal growth stages.

Because surface defects in nanostructures can dramatically change the optical, electrical, and physical properties,[14] it is expected that such a unique structure of ZnO may bring about more efficient ZnO→Eu^{3+} energy transfer compared to analogous bulk materials and conventionally fabricated ZnO nanocrystals. First, the room-temperature photoluminescence (PL) properties of an undoped ZnO sample were examined (Fig. 3a), which featured a broad yellow band centered at 575 nm under UV excitation from a Xe lamp. The yellow band is attributed to oxygen interstitials, O_i, which was confirmed by green emission (ca. 516 nm) from the same sample annealed under a H_2/Ar stream (see Supporting Information, Fig. 3s).

Next, the PL properties of ZnO:Eu samples were measured, and they exhibited a broad yellow band with a maximum at 595 nm and intense red emission of Eu^{3+} under UV excitation ($E > E_g$, Fig. 3b). Eu doping shifts the emission color from yellow to orange (i.e., from (0.42, 0.47) to (0.51, 0.44) in the CIE-1931 color map). The yellow band, which is red-shifted 0.073 eV relative to the undoped sample, is attributed to the transition between O_i[15] and a shallow donor level that may be brought about by Eu doping. The red Eu^{3+} emission, whose intensity is comparable to intrinsic yellow emission, indicates efficient ZnO→Eu^{3+} energy transfer that is never observed in singly Eu^{3+}-doped bulk or nanocrystalline ZnO.[9,11] Moreover, the shape of the UV range of excitation spectra (Fig. 3d) is well-matched to undoped ZnO, which confirms energy transfer from UV-generated delocalized electron and hole pairs in a ZnO nanosheet to Eu^{3+}.[16] However, the UV-excited Eu^{3+} emission exhibits obvious difference from the 464-nm-excited Eu^{3+} emission (Fig. 3c), indicating the difference in Eu^{3+} ions that participate in the two types of emission. The 464 nm photon, which is resonant with the Eu^{3+} $^7F_0$–$^5D_2$ transition, can unselectively excite Eu^{3+} throughout the ZnO nanosheet; as a result, only part of the Eu^{3+} ions are active in UV-excited emission, whereas the 464-nm-excited emission is the summation of emissions over all Eu^{3+} ions. For convenience, Eu^{3+} ions that are active or inactive in UV-excited emission can be named as "Eu_a^{3+}" or "Eu_i^{3+}", respectively.

It was established that Eu^{3+} emission always relates to the charge-transfer state, and the ground-state energy level of Eu^{2+} should be below the bottom of the CB.[7] In spite of the high crystalline quality of ZnO nanosheets (Fig. 2e), the multiposition of Eu^{3+} is inevitable, such as Eu^{3+} in defect complexes and Eu^{3+} at surface layer or inner layers. Though special techniques are required to identify Eu^{3+} defect complexes, based on the following analysis it is believed that Eu_a^{3+} and Eu_i^{3+} correspond to Eu^{3+} ions at the surface and inner layers, respectively. In the homogeneous inner layer of a ZnO nanosheet, where defects and energy levels resemble bulk and microcrystalline ZnO, the ground-state level of Eu^{2+} is higher or equal to the bottom of the CB, and poor ZnO→Eu^{3+} energy transfer is expected. Furthermore, in GaN:Eu where Eu^{3+} ions occupy Ga^{3+} sites (C_{3v}), Eu^{3+} emission spectra resemble the 464-nm-excited Eu_i^{3+} emission (Table 1),[1] indicating that Eu_i^{3+} ions stay in sites that do not

ADVANCED MATERIALS

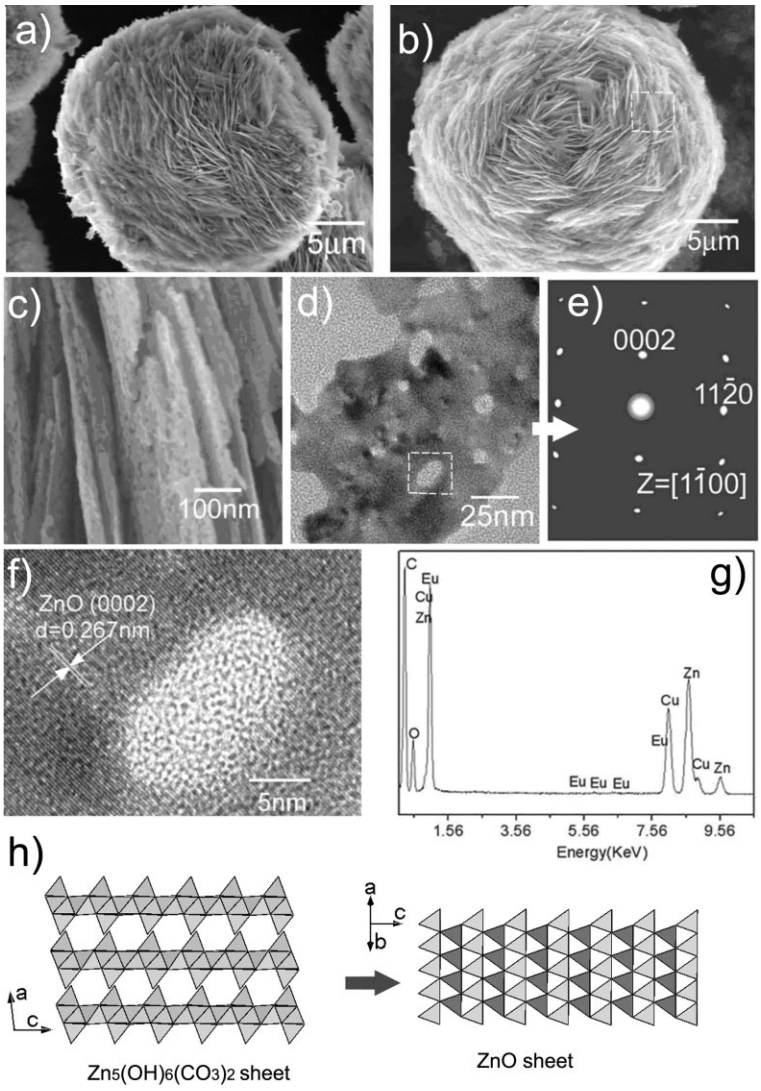

Figure 2. Field-emission scanning electron microscopy (FESEM) and transmission electron microscopy (TEM) images of the as-prepared samples. a) FESEM image of a Eu^{3+}-doped LHZC microsphere; b) FESEM image of a ZnO:Eu microsphere annealed at 400 °C; c) FESEM image of ZnO:Eu nanosheets prepared from microspheres shown in (b); d) typical TEM image of a ZnO:Eu nanosheet; e) selected area electron diffraction (SAED) pattern of ZnO:Eu nanosheets shown in (d); f) HRTEM image of ZnO:Eu nanosheets shown in (d); g) typical energy dispersive X-ray (EDX) spectrum obtained from ZnO:Eu nanosheets, indicating the presence of Eu. In (a)–(g), the Eu^{3+} doping concentration was 0.5 %. h) Schematic illustration of the LHZC to ZnO nanosheet conversion.

deviate far from ideal Zn^{2+} sites (C_{3v}). In contrast, the crystal field suffered by Eu^{3+} ions in the surface layer might be changed from structural relaxation.[17] In the surface layer of the nanosheet, the electron depletion layer, band structure, and positions of Eu^{3+} 4f levels relative to the valence band (VB) and CB are slightly different from bulk ZnO.[5] More significantly, a certain surface defect that closely relates to the [1$\bar{1}$00] surface of the ZnO nanosheet might couple with Eu^{3+} to form a complex, in which the Eu^{2+} ground state level is just below the bottom of the CB. Consequently, the photon-generated free charge carriers can be effectively trapped, and energy is transferred to the coupled Eu_a^{3+} ion via a charge-transfer process.[18]

However, the increase in the Eu^{3+} concentration does not enhance the intensity of UV-excited Eu^{3+} emission (Fig. 3b), and the percentage of UV-excited Eu_a^{3+} emission over the 464-nm-excited emission reduces gradually as the Eu^{3+} concentration increases from 0.1 to 0.7 % (Fig. 3d), suggesting that the number of Eu_a^{3+} ions is not the key factor contributing to the intensity of UV-excited Eu_a^{3+} emission. As discussed above, UV and 464-nm-excited Eu^{3+} emissions follow different PL mechanisms: UV-excited Eu_a^{3+} emission closely relates to charge-carrier trapping by the coupled surface defect and energy transfer to Eu_a^{3+}, but 464-nm-excited Eu^{3+} emission merely depends on the optical absorption of 464 nm photons and radiative 4f–4f transitions within Eu^{3+} ions. In addition, as the doping concentration of Eu^{3+} increases, a gradual decrease was observed in the integration area ratio of self-activated (SA) yellow emission versus exciton emission (Fig. 4), which may originate from the competition of Eu_a^{3+} with oxygen interstitial defects in capturing photon-generated charge carriers. Following the PL model of GaN:Eu^{3+} [1] and rare-earth activators in II-VI semiconductors,[18] the schematic mechanism of UV-excited Eu^{3+} emission in the surface layer of a ZnO nanosheet is illustrated in Scheme 1.

Though the nature of defects that stabilize the Eu^{2+} state remains unknown, it is likely they would be found on the nonpolar [1$\bar{1}$00] surface of the ZnO nanosheet, as previous studies on ZnO:Eu nanorods and quantum dots[11] failed to observe appreciable ZnO→Eu^{3+} energy transfer at cryogenic or room temperatures. The UV-excited Eu^{3+} emission was stable after both an oxidizing and reducing heat treatment (see Supporting Information, Fig.3s); as a result, the sur-

Table 1. Positions (nm) of Eu^{3+} emission peaks and assignments under different excitations.Table 1.

Excitation	Emission ion	$^5D_1$–$^7F_0$	$^5D_0$–$^7F_0$	$^5D_0$–$^7F_1$	$^5D_0$–$^7F_2$	$^5D_0$–$^7F_3$	$^5D_0$–$^7F_4$
UV	Eu_a^{3+}		577	589, 595	612, 619	654	
464 nm	Eu_a^{3+}, Eu_i^{3+}	539	578	590, 595	616, 629	659	ca. 700
464 nm	Eu_i^{3+}	539	578	ca. 591	616, 628	659	ca. 700

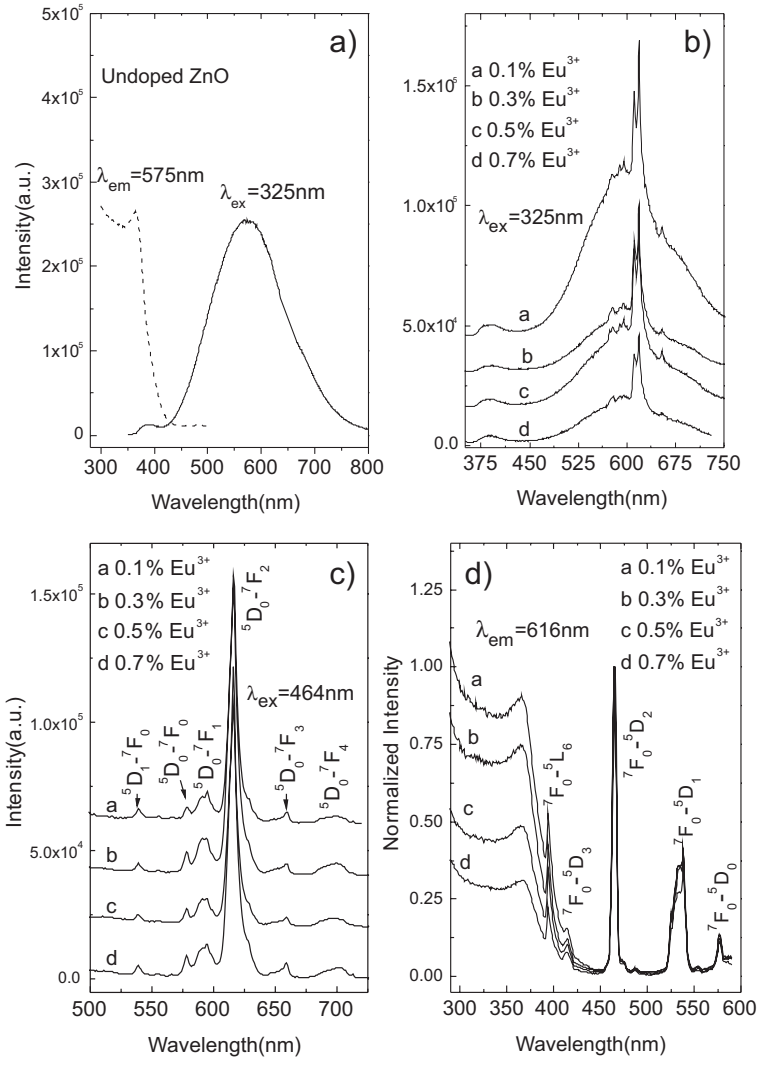

Figure 3. a) Excitation and emission spectra of an undoped ZnO sample. Emission spectra of ZnO:Eu samples under excitation at b) 325 nm and c) 464 nm; d) the excitation spectra of ZnO:Eu (the curves were normalized at 464 nm). The curves in (b) and (c) are stacked for clarity.

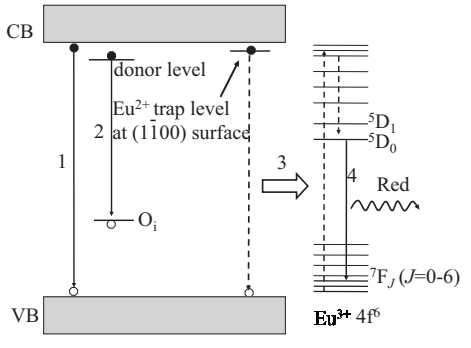

Scheme 1. Schematic of the process of UV-excited Eu^{3+} emission: 1 corresponds to near-band edge exciton emission, 2 is self-activated yellow emission, 3 is the energy transfer from the coupled surface defect to Eu^{3+} ions in the surface layer, and 4 is the $^5D_0$–^7F_J red emission of Eu^{3+}. Charge transfer may be involved within the complex of the coupled surface defect and Eu^{3+} because of the strong intensity of Eu^{3+} emission.

face defects are unlikely to be oxygen vacancies or oxygen interstitial defects. Moreover, the absence of $^5D_1$–$^7F_0$ emission in UV-excited Eu^{3+} emission might be attributed to coordination with CO_3^{2-} or OH^- anions, for which the phonon energy is as high as 1450 and 3100–3400 cm^{-1}, respectively. Consequently, residual CO_3^{2-} or OH^- anions at the nonpolar [1$\bar{1}$00] surface might couple with Eu^{3+} and stabilize the Eu^{2+} level just below the CB of ZnO. The density, charge-carrier trapping rate, and energy-transfer rate of the trap center determine the intensity of UV-excited Eu^{3+} emission, which is in competition with self-activated yellow emission. It is expected that the increase in the density of trap centers and energy-transfer rate will enhance the intensity of UV-excited Eu^{3+} emission in ZnO.

In conclusion, efficient UV-excited Eu^{3+} emission was observed in nanosheet-assembled ZnO:Eu microspheres. The ZnO:Eu microspheres, which consist of crystalline ZnO nanosheets, were fabricated by using layered $Zn_5(OH)_6(CO_3)_2$ as a self-templating precursor and pyrolysis. Eu^{3+} ions were successfully doped into ZnO, and for the first time efficient ZnO→Eu^{3+} energy transfer at room temperature was observed in nanostructures. The UV-excited Eu^{3+} emission is attributed to Eu^{3+} ions in the surface layer of a ZnO nanosheet, where appropriate surface defects may couple with Eu^{3+} to form a complex and facilitate the ZnO→Eu^{3+} energy transfer. More efficient Eu^{3+} emission is expected by the rational control of the density and nature of trap centers in ZnO:Eu nanostructures. This work not only provides an intense red emission component, which had been lacking in designing ZnO-based full-color display devices, but also proves the possibility of realizing efficient RE^{3+} 4f–4f emission in ZnO nanostructures that could be utilized in various optoelectric applications. Moreover, because of the surface-related nature, such ZnO:Eu nanostructure have special potential in designing environmental sensors and biomolecule labeling devices.

Experimental

Samples were fabricated under mild hydrothermal conditions and heat treatment. Analytical pure $Zn(NO_3)_2{\cdot}6\ H_2O$, Eu_2O_3, and urea were used as starting materials. Eu_2O_3 was dissolved in dilute nitric acid to obtain a 0.02 M europium nitrate aqueous solution. $Zn(NO_3)_2{\cdot}6\ H_2O$ was dissolved in deionized water, and a europium nitrate solution and urea were added to this solution in a molar ratio of Zn^{2+}/Eu^{3+}/urea of 1:*x*:10 (*x* = 0, 0.001, 0.003, 0.005, 0.007), and the concentration of metal ions was adjusted to 0.10 M. Next, the mixed solution (pH 6.5) was transferred into a 60 mL Teflon-lined stainless steel autoclave that was filled nearly 80 %. Hydrothermal treatments were carried out at 120 °C for 12 h and the material was then cooled; the final pH was 9.0. After washing with deionized water and ethanol, the precipitate was dried at 60 °C and annealed at 400 °C in air or Ar/

ADVANCED MATERIALS

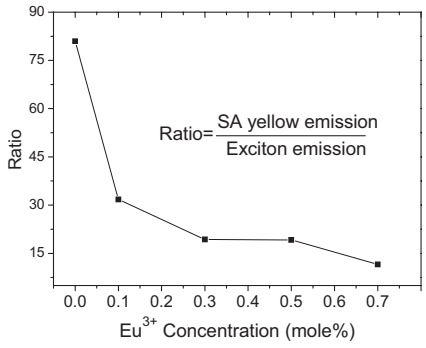

Figure 4. The integration area ratio of self-activated (SA) yellow emission versus the exciton emission in ZnO:Eu^{3+} samples with different doping concentrations.

H_2 gas for 2 h. The products were characterized by XRD (Philips X'pert PRO diffractometer, Cu Kα radiation), XPS (VG ESCALAB 250, Al Kα), scanning electron microscopy (SEM, Sirion 200), high-resolution transmission electron microscopy (HRTEM, JEOL 2010, 200 kV), and energy dispersive X-ray (EDX) analysis attached to a transmission electron microscope. The room-temperature emission and excitation spectra were recorded on a Fluorolog-3 Jobin Yvon spectrophotometer using a 450 W Xe lamp as the excitation source.

Received: October 23, 2006
Revised: August 31, 2007

[1] a) H. J. Lozykowski, *Phys. Rev. B* **1993**, *48*, 17 758; b) J. Sawahata, H. Bang, J. Seo, K. Akimoto, *Sci. Technol. Adv. Mat.* **2005**, *6*, 644. c) R. Kudrawiec, M. Nyk, A. Podnorodecki, J. Misiewicz, W. Strek, M. Wolcyrz, *Appl. Phys. Lett.* **2006**, *88*, 061 916; d) A. Svane, N. E. Christensen, L. Petit, Z. Szotek. W. M. Tmmerman, *Phys. Rev. B* **2006**, *74*, 165 204.

[2] M. Klik, T. Gregorkiewicz, I. Bradley, J-P. Wells, *Phys. Rev. Lett.* **2002**, *89*, 227 401.

[3] H. Yan, J. Johnson, M. Law, R. He, K. Knutsen, J. R. McKinney, J. Pham, R. Saykally, P. Yang, *Adv. Mater.* **2003**, *15*, 1907.

[4] B. C. Cheng, Y. H. Xiao, G. S. Wu, L. D. Zhang, *Adv. Funct. Mater.* **2004**, *14*, 913.

[5] K. Vanheusden, C. H. Seager, W. L. Warren, D. R. Tallant, J. A. Voigt, *Appl. Phys. Lett.* **1996**, *68*, 403.

[6] a) Y. Hayashi, H. Narahara, T. Uchida, T. Noguchi, S. Ibuki, *Jpn. J. Appl. Phys.* **1995**, *34*, 1878; b) Y. K. Park, J. I. Han, M. G. Kwak, H. Yang, S. H. Ju. W. S. Cho, *Appl. Phys. Lett.* **1998**, *72*, 668; c) C. C. Yang, S. Y. Cheng, H. Y. Lee, S. Y. Chen, *Ceram. Int.* **2006**, *32*, 37.

[7] a) P. Dorenbos, E. van der Kolk, *Appl. Phys. Lett.* **2006**, *89*, 061 122. b) P. Dorenbos, E. van der Kolk, *Proc. SPIE* **2007**, *6473*, 647 313.

[8] a) G. P. Morgan, W. M. Yen, *Laser Spectroscopy of Solids II*, Springer-Verlag, New York **1989**, p. 77; b) A. van Dijken, E. A. Meulemkamp, D. Vanmaekelbergh, A. Merjerink, *J. Lumin.* **2000**, *87–89*, 454.

[9] a) D. Prezzi, T. Eberlein, J.-S. Filhol, R. Jones, M. J. Shaw, P. R. Briddon, S. Öberg, *Phys. Rev. B* **2004**, *69*, 193 202. b) V. X. Quang, N. G. Liem, N. C. Thanh, T. V. Chuong, L. L. Thanh, *Phys. Status Solidi A* **1983**, *78*, K161; c) W. Y. Jia, K. Monge, F. Fernandez, *Opt. Mater.* **2003**, *23*, 27.

[10] a) Y. Harada, S. Hashimoto, *Phys. Rev. B* **2003**, *68*, 045 421. b) J. Grabowska, A. Meaney, K. K. Nanda, J. P. Mosnier, M. O. Henry, J. R. Duclere, E. McGlynn, *Phys. Rev. B* **2005**, *71*, 115 439.

[11] a) R. N. Bhargava, V. Chhabra, T. Som, A. Ekimov, N. Taskar, *Phys. Status Solidi B* **2002**, *229*, 897; b) M. Abdullah, T. Morimoto, K. Okuyama, *Adv. Funct. Mater.* **2003**, *13*, 800. c) A. Ishizumi, Y. Kanemitsu, *Appl. Phys. Lett.* **2005**, *86*, 253 106. d) A. Ishizumi, Y. Taguchi, H. Yamamoto, Y. Kanemitsu, *Thin Solid Films* **2005**, *486*, 50; e) S. Gao, H. Zhang, R. Deng, X. Wang, D. Sun, G. Zheng, *Appl. Phys. Lett.* **2006**, *89*, 123 125.

[12] a) E. Hosono, S. Fujihara, I. Honma, H. S. Zhou, *Adv. Mater.* **2005**, *17*, 2091; b) K. Kakiuchi, E. Hosono, T. Kimura, H. Imai, S. Fujihara, *J. Sol-Gel Sci. Technol.* **2006**, *39*, 63.

[13] a) S. Ghose, *Acta Crystallogr.* **1964**, *17*, 1051; b) H. Sawada, R. Wang, A. W. Sleight, *J. Solid State Chem.* **1996**, *122*, 148.

[14] W. P. Halperin, *Rev. Mod. Phys.* **1986**, *58*, 532.

[15] a) L. E. Greene, M. Law, J. Goldberger, F. Kim, J. C. Johnson, Y. Zhang, R. J. Saykally, P. Yang, *Angew. Chem. Int. Ed.* **2003**, *115*, 3139; b) J. W. P. Hsu, D. R. Tallant, R. L. Simpson, N. A. Missert, R. G. Copeland, *Appl. Phys. Lett.* **2006**, *88*, 252 103.

[16] H. Kühne, G. Weiser, E. I. Terukov, A. N. Kusnetsov, V. Kh. Kudoyarova, *J. Appl. Phys.* **1999**, *86*, 896.

[17] I. Ivanov, J. Pollmann, *Phys. Rev. B* **1981**, *24*, 7275.

[18] R. Boyn, *Phys. Status Solidi B* **1988**, *148*, 11.

